

Mutually Causal Semantic Distillation Network for Zero-Shot Learning

Shiming Chen^{1,2} · Shuhuang Chen^{1,2} · Guo-Sen Xie³ · Xinge You^{1,2}

¹ Huazhong University of Science and Technology, Wuhan, China

² National Anti-Counterfeit Engineering Research Center, Wuhan, China

³ Nanjing University of Science and Technology, Nanjing, China

{gchenshiming,gsxiehm}@gmail.com

{shuhuangchen,youxcg}@hust.edu.cn

the date of receipt and acceptance should be inserted later

Abstract Zero-shot learning (ZSL) aims to recognize the unseen classes in the open-world guided by the side-information (*e.g.*, attributes). Its key task is how to infer the latent semantic knowledge between visual and attribute features on seen classes, and thus conducting a desirable semantic knowledge transfer from seen classes to unseen ones. Prior works simply utilize unidirectional attention within a weakly-supervised manner to learn the spurious and limited latent semantic representations, which fail to effectively discover the intrinsic semantic knowledge (*e.g.*, attribute semantic) between visual and attribute features. To solve the above challenges, we propose a mutually causal semantic distillation network (termed **MSDN++**) to distill the intrinsic and sufficient semantic representations for ZSL. MSDN++ consists of an attribute→visual causal attention sub-net that learns attribute-based visual features, and a visual→attribute causal attention sub-net that learns visual-based attribute features. The causal attentions encourages the two sub-nets to learn causal vision-attribute associations for representing reliable features with causal visual/attribute learning. With the guidance of semantic distillation loss, the two mutual attention sub-nets learn collaboratively and teach each other throughout the training process. Extensive experiments on three widely-used benchmark datasets (*e.g.*, CUB, SUN, AWA2, and FLO) show that our MSDN++ yields significant improvements over the strong baselines, leading to new state-of-the-art performances.

Keywords Open-World Visual Recognition · Zero-Shot Learning · Mutual Semantic Distillation · Attribute localization

1 Introduction and Motivation

Visual recognition is a critical task in computer vision, which has attracted significant attention in recent years due to its numerous applications in real-world, *e.g.*, autonomous driving (Hu et al, 2023), smart healthcare (Bai et al, 2021), and intelligent surveillance (Collins et al, 2000). Over the past decade, deep learning techniques and large-scale datasets have contributed to remarkable advancements in the performance of visual recognition systems (He et al, 2016; Wang et al, 2020b,a). However, existing visual models are often limited by their closed-world assumptions, where all possible classes are known in advance, and all data is given at once. Such assumptions are not applicable in practical scenarios, where novel or previously unseen classes can arise, and data may be continually coming or decentralized due to data privacy concerns. For example, an autonomous vehicle encounters new traffic patterns, a medical AI system detects new diseases, or an intelligent system encounters a criminal wearing a new type of disguise or clothing. Based on the prior knowledge of seen classes, humans have a remarkable ability to recognize new concepts (classes) using shared and distinct attributes of both seen and unseen classes (Lampert et al, 2009).

Analogously, zero-shot learning (ZSL) is proposed under a challenging image classification setting to mimic the human cognitive process (Larochelle et al, 2008; Palatucci et al, 2009). ZSL aims to tackle the unseen class recognition problem by transferring knowledge from seen classes to unseen ones. It is usually based on the assumption that both seen and unseen classes can be described through the shared semantic descriptions (*e.g.*, attributes) (Lampert et al, 2014). Based on the classes classified in the testing phase, ZSL methods can be grouped into conventional ZSL (CZSL) and generalized ZSL (GZSL) (Xian et al, 2017), where CZSL aims to predict unseen classes, while GZSL can predict both

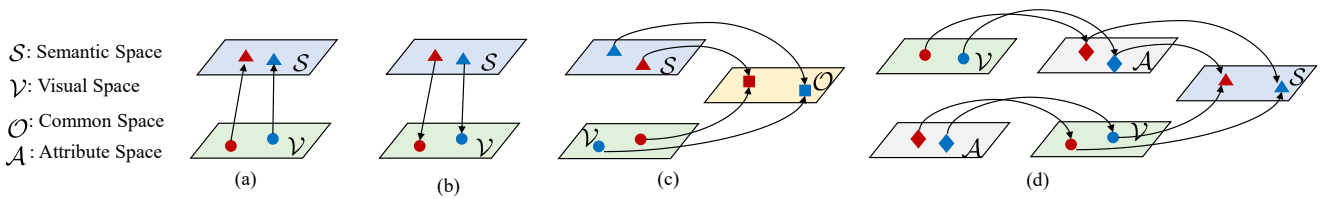


Fig. 1: Four investigated ZSL paradigms. (a) Embedding-based method. (b) Generative method. (c) Common space learning method. (d) Ours proposed mutually causal semantic distillation network (MSDN++). The semantic space \mathcal{S} is represented by the class semantic vector annotated by humans based on the attribute descriptions. The visual space \mathcal{V} is learned by a network backbone (e.g., ResNet101 (He et al, 2016)). The common space \mathcal{O} is a shared latent space between visual mapping and semantic mapping. The attribute space \mathcal{A} is learned by a language model (e.g., Glove (Pennington et al, 2014)). Filled triangles, circles, squares and diamonds denote the sample features in \mathcal{S} , \mathcal{V} , \mathcal{O} and \mathcal{A} , respectively.

seen and unseen ones. Since GZSL is more realistic and challenging (Pourpanah et al, 2020), some ZSL methods only focus on the GZSL setting (Liu et al, 2018; Han et al, 2020, 2021; Chen et al, 2021b; Huynh and Elhamifar, 2020a). In this work, we sufficiently evaluate our method both in the two settings.

In the ZSL, an unseen sample shares different partial information with a set of samples of seen classes, and this partial information is represented as the abundant semantic knowledge of attributes (e.g., “bill color yellow”, “leg color red” on CUB dataset) (Wang et al, 2021b; Chen et al, 2022a, 2023a, 2024c). To this end, the key challenge of ZSL is how to infer the latent semantic knowledge between visual and attribute features on seen classes, allowing desirable knowledge transfer to unseen classes for effective visual-semantic match. Targeting on this goal, some attention-based ZSL methods (Xie et al, 2019, 2020; Zhu et al, 2019; Xu et al, 2020; Liu et al, 2021; Chen et al, 2024b, 2022a, 2023a, 2025) take attention mechanism to discover discriminative part/fine-grained visual features, which match the semantic representations more accurately, enabling significant ZSL performance. Unfortunately, i) they simply utilize unidirectional attention, which only focuses on limited semantic alignments between visual and attribute features without any further sequential learning; ii) they learn the attention with an attention modules simply supervised by the classical loss function, which only explicitly supervises the final prediction but ignores the causality between the prediction and attention. As such, prior attention-based methods can only discover the spurious and limited semantic representations between visual and attribute features, resulting in undesirable semantic knowledge transfer in the ZSL.

In light of the above observations, we propose a mutually causal semantic distillation network (termed MSDN++), to explore the intrinsic semantic knowledge between visual and attribute features for advancing ZSL, as shown in Fig. 1 (d). The core idea is to evaluate the quality of attentions by comparing the effects of facts (i.e., the learned attentions)

and the intervention (i.e., uncorrected attentions) on the final prediction. Then, we maximize the effects between the two attentions (i.e., effect in causal inference (Pearl, 2009; Pearl et al, 2016; Li et al, 2024)) to encourage the network to learn more effective visual attentions and reduce the effects of bias of training data. Meanwhile, this causal mechanism is incorporated into the mutually semantic distillation network (i.e., MSDN (Chen et al, 2022b)), enabling the network to discover the intrinsic and more sufficient semantic knowledge for feature representations.

Specifically, MSDN++ consists of an attribute→visual causal attention sub-net, which learns attribute-based visual features with attribute-based/causal visual learnings, and a visual→attribute causal attention sub-net, which learns visual-based attribute features via visual-based/causal attribute learnings. The causal attentions encourages the two sub-nets to learn causal vision-attribute associations for representing reliable features. Meanwhile, these two mutual attention sub-nets act as a teacher-student network for guiding each other to learn collaboratively and teaching each other throughout the training process. As such, MSDN++ can explore the most matched attribute-based visual features and visual-based attribute features, enabling to effectively distill the intrinsic semantic representations for desirable knowledge transfer from seen to unseen classes. Specifically, each causal attention sub-net is optimized with an attribute-based cross-entropy loss with self-calibration (Zhu et al, 2019; Huynh and Elhamifar, 2020a; Xu et al, 2020; Liu et al, 2021; Chen et al, 2022a), attribute regression loss, and causal loss. To enable mutual learning between the two sub-nets, we further introduce a semantic distillation loss that aligns each other’s class posterior probabilities. Extensive experiments well demonstrate the superiority of MSDN++ over the existing state-of-the-art methods.

A preliminary version of this work was presented as a CVPR 2022 conference paper (termed MSDN (Chen et al, 2022b)). In this version, we strengthen the work from three aspects: i) We further analyze the limitations of existing

attention-based ZSL methods, which simply utilize unidirectional attention in a weakly-supervised manner to learn the spurious and limited latent semantic representations. As such, they fail to effectively discover the intrinsic and sufficient semantic knowledge between visual and attribute features. ii) We propose two novel sub-nets to equip MSDN with causal attentions, which enable the model to learn causal vision-attribute associations for representing reliable features. iii) We conduct substantially more experiments to demonstrate the effectiveness of the proposed methods and verify the contribution of each component.

The main contributions of this paper are summarized as follows:

- We propose a mutually causal semantic distillation network, termed MSDN++, which distills the intrinsic and sufficient semantic representations for effective knowledge transfer of ZSL.
- We deploy causal visual learning and causal attribute learning to encourage MSDN++ to learn the causal vision-attribute associations for representing reliable features with good generalization.
- We introduce a semantic distillation loss to enable mutual learning between the attribute→visual causal attention sub-net and visual→attribute causal attention sub-net in MSDN++, encouraging them to learn attribute-based visual features and visual-based attribute features by distilling the intrinsic semantic knowledge for semantic embedding representations.
- We conduct extensive experiments to demonstrate that our MSDN++ achieves significant performance gains over the strong ZSL baselines on four benchmarks, *i.e.*, CUB (Welinder et al, 2010), SUN (Patterson and Hays, 2012), AWA2 (Xian et al, 2017), and FLO Nilsback and Zisserman (2008).

The rest of this paper is organized as follows. Section 2 discusses related works. The proposed MSDN++ is illustrated in Section 3. Experimental results and discussions are provided in Section 4. Finally, we draw a conclusion in Section 5.

2 Related Work

2.1 Zero-Shot Learning

ZSL (Song et al, 2018; Li et al, 2018; Xian et al, 2018, 2019; Yu et al, 2020; Min et al, 2020; Han et al, 2021; Chen et al, 2021b; Chou et al, 2021) transfer semantic knowledge from seen classes to unseen ones by learning a mapping between the visual and attribute/semantic domains. There are several ZSL approaches targeting this goal, *i.e.*, embedding-based methods, generative methods, and common space

learning-based methods. As shown in Fig. 1 (a), embedding-based methods learn a visual→semantic mapping for visual-semantic interaction by mapping the visual features into the semantic space (Romera-Paredes and Torr, 2015; Akata et al, 2016; Chen et al, 2018; Xie et al, 2019; Xu et al, 2020). Generative ZSL methods have been introduced to learn a semantic→visual mapping to generate visual features of unseen classes (Arora et al, 2018; Schönfeld et al, 2019; Xian et al, 2018; Li et al, 2019a; Yu et al, 2020; Shen et al, 2020; Vyas et al, 2020; Narayan et al, 2020; Chen et al, 2021b, 2023b) for data augmentation, shown in Fig. 1 (b). Generative ZSL methods usually base on variational autoencoders (VAEs) (Arora et al, 2018; Schönfeld et al, 2019), generative adversarial nets (GANs) (Xian et al, 2018; Li et al, 2019b; Yu et al, 2020; Keshari et al, 2020; Vyas et al, 2020; Chen et al, 2021b, 2025), or generative flows (Shen et al, 2020). As shown in Fig. 1 (c), common space learning is also employed to learn a common representation space for interaction between visual and semantic domains (Frome et al, 2013; Tsai et al, 2017; Schönfeld et al, 2019; Chen et al, 2021c). However, these methods still usually perform relatively sub-optimal results, since they cannot capture the subtle differences between seen and unseen classes. As such, attention-based ZSL methods (Xie et al, 2019, 2020; Zhu et al, 2019; Xu et al, 2020; Liu et al, 2021; Chen et al, 2024b, 2022a) utilize attribute descriptions as guidance to discover the more discriminative fine-grained features.

However, they simply utilize unidirectional attention in a weakly-supervised manner, which only focuses on spurious and limited semantic alignments between visual and attribute features without any further sequential learning. As such, the existing method fails to explore the intrinsic and sufficient semantic representations between visual and attribute features for semantic knowledge transfer of ZSL. To tackle this challenge, we will introduce a novel ZSL method based on the mutually semantic distillation learning and causal attention mechanism.

2.2 Knowledge Distillation

To compress knowledge from a large teacher network to a small student network, knowledge distillation was proposed (Hinton et al, 2015). Recently, knowledge distillation has been extended to optimize small deep networks starting with a powerful teacher network (Romero et al, 2015; Parisotto et al, 2016). By mimicking the teacher’s class probabilities and/or feature representation, distilling models convey additional information beyond the conventional supervised learning target (Zhang et al, 2018; Zhai et al, 2020). Motivated by these, we design a mutually semantic distillation network to learn the intrinsic semantic knowledge by semantically distilling intrinsic knowledge. The mutually semantic distillation network consists of attribute→visual attention and

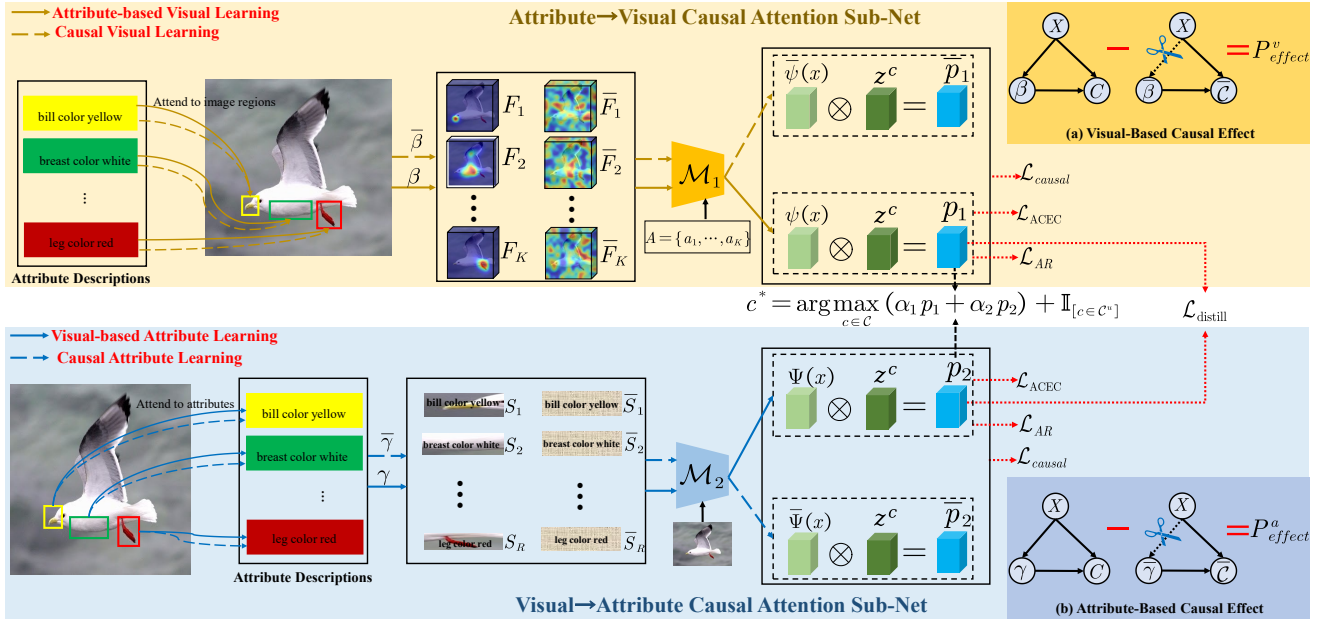


Fig. 2: The pipeline of MSDN++. MSDN++ consists of an attribute→visual causal attention sub-net (AVCA) and visual→attribute causal attention sub-net (VACA). AVCA learns the attribute-based visual features F with attribute-based visual learning and causal visual learning, while VACA discovers the vision-based attribute features S with vision-based attribute learning and causal attribute learning. Then, two mapping functions \mathcal{M}_1 and \mathcal{M}_2 map the visual features and attribute features into semantic space as semantic representations $\psi(x)$ and $\Psi(x)$, respectively. A semantic distillation loss $\mathcal{L}_{distill}$ to match the probability estimates of the two sub-nets for semantic distillation (i.e., p_1 and p_2), enabling MSDN++ to learn intrinsic semantic knowledge. During inference, we fuse the predictions of the two sub-nets to take full use of the complementary semantic representations.

visual→attribute attention sub-nets, which act as a teacher-student network to learn collaboratively and teach each other.

2.3 Causal Inference in Vision

Causality typically includes two inferences, i.e., intervention inference and counterfactual inference (Pearl, 2009; Pearl et al, 2016), and it has been successfully applied in several areas of artificial intelligence, such as explainable machine learning (Lv et al, 2022), natural language processing (Wood-Doughty et al, 2018), reinforcement learning (Kallus and Zhou, 2018) and adversarial learning (Zhang et al, 2021). Since causal representation can alleviate the effects of dataset bias, it served as an effective tool in vision tasks (Yue et al, 2020; Rao et al, 2021; Tang et al, 2020; Chen et al, 2021a; Wang et al, 2021a; Yang et al, 2021; Li et al, 2023a). For example, Chen et al. (Chen et al, 2021a) employed a counterfactual analysis method to alleviate the over-dependence of environment bias and highlight the trajectory clues itself. Wang et al. (Wang et al, 2021a) introduced causal intervention into the visual model to learn causal features that are robust in any confounding context. Li et al. (Li et al, 2023a)

and Yue et al. (Yue et al, 2020) bring the causal inference into few-shot learning and obtain significant performances. In ZSL, there are clear projection domain shifts between seen and unseen classes (Fu et al, 2015; Chen et al, 2023b), e.g., the attribute of "has tail" is different for horse (seen class) and pig (unseen class), which inevitably leads the attention model to learn the spurious associations between visual and attribute features. Accordingly, we deploy causal attention via intervention inference to enable the ZSL model to learn causal features, which are robust to visual bias. Accordingly, the generalization of ZSL can be improved.

3 Mutually Causal Semantic Distillation Network

Notation. Assume that the training data $\mathcal{D}^s = \{(x_i^s, y_i^s)\}$ has C^s seen classes, where $x_i^s \in \mathcal{X}^s$ denotes the visual sample i , and $y_i^s \in \mathcal{Y}^s$ is the corresponding class label. Another set of unseen classes $\mathcal{D}^u = \{(x_i^u, y_i^u)\}$ has C^u classes, where $x_i^u \in \mathcal{X}^u$ are the unseen class samples, and $y_i^u \in \mathcal{Y}^u$ are the corresponding labels. A set of class semantic vectors/prototypes (semantic value annotated by humans according to attributes) of the class $c \in \mathcal{C}^s \cup \mathcal{C}^u = \mathcal{C}$ with

K attributes $z^c = [z_1^c, \dots, z_K^c]^\top = \phi(y)$ (where $\phi(\cdot)$ is a mapping function to bridge the z^c and y) support knowledge transfer from seen classes to unseen ones. Here, the semantic attribute vectors of each attribute $A = \{a_1, \dots, a_K\}$ learned by GloVe (Pennington et al, 2014), it essentially is the attribute features.

Overview. As illustrated in Fig. 2, our MSDN++ includes an attribute →visual causal attention sub-net (AVCA) and visual → attribute causal attention sub-net (VACA). Under the constraint of attribute-based cross-entropy loss with self-calibration, attribute-regression loss, and causal loss, the AVCA and VACA attempt to learn attribute-based causal visual features with causal visual learning visual-based causal attribute representations using causal attribute learning, respectively. A semantic distillation loss encourages the two mutual causal attention sub-nets to learn collaboratively and teach each other throughout the training process. During Inference, we fuse the predictions of AVCA and VACA to make use the complementary semantic knowledge between the two sub-nets.

3.1 Attribute→Visual Causal Attention Sub-net

Existing methods demonstrate that learning the fine-grained features for attribute localization is important in ZSL (Xie et al, 2019, 2020; Zhu et al, 2019; Xu et al, 2020). In the first component of our MSDN++, we proposed an AVCA, which localizes the most relevant image regions corresponding to the attributes to extract attribute-based visual features from a given image for each attribute. AVCA includes two streams, *i.e.*, attribute-based visual learning and causal visual learning. Attribute-based visual learning stream learns attribute-based visual features, which is strengthened with causality using a causal visual learning stream further.

3.1.1 Attribute-Based Visual Learning

Attribute-based visual learning involves two inputs: a set of visual features of the image $V = \{v_1, \dots, v_R\}$ (where R is the number of regions), such that each visual feature encodes a region in an image, and a set of semantic attribute vectors $A = \{a_1, \dots, a_K\}$. AVCA attends to image regions with respect to each attribute and compares each attribute to the corresponding attended visual region features to determine the importance of each attribute. For the k -th attribute, its attention weight of focusing on the r -th region of one image is defined as:

$$\beta_k^r = \frac{\exp(a_k^\top W_1 v_r)}{\sum_{k=1}^K \exp(a_k^\top W_1 v_r)}, \quad (1)$$

where W_1 is a learnable matrix to calculate the visual feature of each region and measure the similarity between each

semantic attribute vector. As such, we get a set of attention weights $\{\beta_k^r\}_{r=1}^R$.

AVCA then learns the attribute-based visual features for each attribute based on the attention weights. For example, AVCA obtains the k -th attribute-based visual feature F_k , which is relevant to the k -th attribute a_k . It is formulated as:

$$F_k = \sum_{r=1}^R \beta_k^r v_r. \quad (2)$$

Intuitively, F_k captures the visual evidence to localize the corresponding semantic attribute in the image. If an image has an obvious attribute a_k , the model will assign a high positive score to the k -th attribute. Otherwise, the model will assign a low score to the k -th attribute. Thus, we get a set of attribute-based visual features $F = \{F_1, F_2, \dots, F_K\}$.

After obtaining the attribute-based visual features, AVCA further maps them into the semantic embedding space using a mapping function \mathcal{M}_1 . To encourage the mapping to be more accurate, the semantic attribute vectors $A = \{a_1, a_2, \dots, a_K\}$ are served as support. Specifically, \mathcal{M}_1 matches the attribute-based visual feature F_k with its corresponding semantic attribute vector a_k , formulated as:

$$\psi_k = \mathcal{M}_1(F_k) = a_k^\top W_2 F_k, \quad (3)$$

where W_2 is an embedding matrix that maps F into the semantic space. Essentially, ψ_k is an attribute score that represents the confidence of having the k -th attribute in a given image. Finally, AVCA obtains a mapped semantic embedding $\psi(x) = \{\psi_1, \psi_2, \dots, \psi_K\}$ for each image.

Accordingly, the final prediction can be formulated as:

$$p_1 = \{\psi(x_i) \times z^1, \dots, \psi(x_i) \times z^K\}. \quad (4)$$

Notably, p_1 is the observation prediction of sample x_i in AVCA.

3.1.2 Causal Visual Learning

There are clear projection domain shifts between seen and unseen classes in ZSL (Fu et al, 2015; Chen et al, 2023b), which inevitably results in the attention model to learn the spurious associations between visual and attribute features of seen and unseen classes. Accordingly, we deploy causal visual learning to strengthen the attribute-based visual features with causality, enabling AVCA to learn attribute-based causal visual features.

Visual Causal Graph. We reformulate the attribute-based visual learning with a visual causal graph $\mathcal{G}_v = \{\mathcal{V}_v, \mathcal{E}_v\}$. Each variable in the graph has a corresponding node in \mathcal{V}_v , and the causal links \mathcal{E}_v describe how these variables interact with each other. As shown in Fig. 2(a), the nodes \mathcal{V}_v in \mathcal{G}_v are represented by visual features X , the learned attention maps β , and final prediction \mathcal{C} . $(X, \beta) \rightarrow \mathcal{C}$ denotes the

visual features and attention maps jointly determine the final predictions, where we call node X is the causal parent of β and \mathcal{C} is the causal child of X and β .

Visual-Based Causal Effect. Attribute-based visual learning optimizes the attention by only supervising the final prediction \mathcal{C} , which ignores how the learned attention maps affect the final prediction. In contrast, causal inference (Frappier, 2018) is a good tool to help us analyze the causalities between variables of the model. Inspired by this, we propose to adopt the causality to measure the quality of the learned attention and then improve the model by encouraging the network to produce more influential attention maps. Using the visual causal graph, we can analyze causalities by directly manipulating the values of attention and seeing the effect. The operation is formally called causal intervention, which can be denoted as $do(\cdot)$.

Specifically, we take $do(\beta = \bar{\beta})$ in \mathcal{G}_v to conduct causal intervention, e.g., random attention. Notably, we chose random attention as the counterfactual baseline because it represents a null intervention with minimal structural assumptions. Unlike “learned null attention” (which may still embed dataset biases) or “marginal attention” (which requires estimating a prior distribution from data), random attention is provably independent of both visual inputs and model parameters. This ensures that the intervention $do(\beta = \bar{\beta})$ truly severs the causal link between visual features and attention, fulfilling the do-operator’s requirement of an exogenous manipulation. It provides a clean, unbiased baseline to measure the true causal effect of the learned attention. This means we replace the variable β with the values of $\bar{\beta}$ by cutting-off the link $X \rightarrow \beta$, which without any causal associations with the visual features X . Following the attribute-based visual learning, we can obtain the causal visual features $\bar{F} = \{\bar{F}_1, \bar{F}_2, \dots, \bar{F}_K\}$ and the causal semantic mapped embedding $\bar{\psi}(x) = \{\bar{\psi}_1, \bar{\psi}_2, \dots, \bar{\psi}_K\}$ according to Eq. 2 and Eq. 3, respectively.

Then, the class predictions after intervention $do(\beta = \bar{\beta})$ can be obtained by:

$$P(do(\beta = \bar{\beta}), X = x_i) = \{\bar{\psi}(x_i) \times z^1, \dots, \bar{\psi}(x_i) \times z^C\}. \quad (5)$$

Accordingly, the actual effect of the learned attention on the prediction can be represented by the difference between the observed prediction $p_1 = P(\beta, X = x_i)$ and its causal intervention one $P(do(\beta = \bar{\beta}), X = x_i)$. It is formulated as:

$$P_{effect}^v(x_i) = P(\beta, X = x_i) - P(do(\beta = \bar{\beta}), X = x_i) \quad (6)$$

Because $\bar{\beta}$ is drawn from a uniform distribution (post softmax), it represents a maximally entropic, non-informative attention over regions. Thus, the causal effect captures how much the learned attention improves prediction compared to a completely uninformative one. We also experimented with

other counterfactual distributions (e.g., uniform attention, reversed attention) in Table 4, and results show our model is robust to the choice of $\bar{\beta}$ distribution—as long as it is independent of the input, the causal learning signal remains effective. Therefore, we can use $P_{effect}^v(x_i)$ to evaluate the quality of the learned visual attention and improve the causality of attribute-based visual features.

3.2 Visual→Attribute Causal Attention Sub-net

VACA includes a visual-based attribute learning stream that learns visual-based attribute representations, and a causal attribute learning that enhances the attribute features with causality. Visual-based attribute representations are complementary to the attribute-based visual features, enabling them to calibrate each other. As such, MSDN++ can discover the intrinsic semantic representations between visual and attribute features.

3.2.1 Visual-Based Attribute Learning

Visual-based attribute learning first attends to semantic attributes with respect to each image region. Formally, its attention weights focus on the k -th attribute defined as:

$$\gamma_r^k = \frac{\exp(v_r^\top W_3 a_k)}{\sum_{r=1}^R \exp(v_r^\top W_3 a_k)}, \quad (7)$$

where W_3 is a learnable matrix, which measures the similarity between the semantic attribute vector and each visual region feature. Accordingly, VACA can get a set of attention weights $\{\gamma_r^k\}_{k=1}^K$, which is employed to extract visual-based attribute features, formulated as:

$$S_r = \sum_{k=1}^K \gamma_r^k a_k. \quad (8)$$

Essentially, S_r is the visual-based attribute representation, which is aligned to the F_k . VACA further employs a mapping function \mathcal{M}_2 to map these visual-based attribute features $S = \{S_1, S_2, \dots, S_R\}$ into the semantic space:

$$\hat{\Psi}_r = \mathcal{M}_2(S_r) = v_r^\top W_4 S_r, \quad (9)$$

where W_4 is an embedding matrix. Given a set of $V = \{v_1, \dots, v_R\}$, VACA obtains the mapped semantic embedding $\hat{\Psi}(x) = \{\hat{\Psi}_1, \hat{\Psi}_2, \dots, \hat{\Psi}_R\}$ for the attributes of one image. To enable the learned semantic embedding $\hat{\Psi}(x_i)$ is R -dim to match with the dimension of class semantic vector (K -dim), it is further mapped into semantic attribute space with K -dim, formulated as $\Psi(x_i) = \hat{\Psi}(x_i) \times Att = \hat{\Psi}(x_i) \times (V^\top W_{att} A)$, where W_{att} is a learnable matrix.

Finally, we can get the final prediction with the mapped semantic vectors and class semantic vector:

$$p_2 = \{\Psi(x_i) \times z^1, \dots, \Psi(x_i) \times z^C\}. \quad (10)$$

Essentially, p_2 is the observation prediction of sample x_i in VACA.

3.2.2 Causal Attribute Learning

Similar to AVCA, VACA further improves the causality of visual-based attribute features using causal attribute learning.

Attribute Causal Graph. VACA first formulate a attribute causal graph $\mathcal{G}_a = \{\mathcal{V}_a, \mathcal{E}_a\}$. The graph consists of the corresponding nodes in \mathcal{V}_a , and the causal links \mathcal{E}_a capturing the causal relationships between each other. As shown in Fig. 2(b), the nodes of \mathcal{G}_a are represented by visual features X , the learned attribute attention maps γ , and final prediction \mathcal{C} . $(X, \gamma) \rightarrow \mathcal{C}$ represents the visual features and attribute attention maps jointly determine the final predictions, where we call node X is the causal parent of γ and \mathcal{C} is the causal child of X and γ .

Attribute-Based Causal Effect. Based on the attribute causal graph, we can analyze causalities by directly manipulating the values of attribute attention and see the effect. For example, $do(\gamma = \bar{\gamma})$ in \mathcal{G}_a conduct causal intervention, *e.g.*, random attention. This means we replace the variable γ with the values of $\bar{\gamma}$ by cutting off the link $X \rightarrow \gamma$, which does not have any causal associations with the visual features X . Following the visual-based attribute learning, we can obtain the causal attribute features $\bar{S} = \{\bar{S}_1, \bar{S}_2, \dots, \bar{S}_R\}$, the causal mapped embedding $\bar{\Psi}(x) = \{\bar{\Psi}_1, \bar{\Psi}_2, \dots, \bar{\Psi}_K\}$ and final prediction \bar{p}_2 according to Eq. 8, Eq. 9, and Eq. 10, respectively.

Then, the class predictions based on the causal intervention $do(\gamma = \bar{\gamma})$ is formulated as:

$$C(do(\gamma = \bar{\gamma}), X = x_i) = \arg \max_{c \in \mathcal{C}} \bar{p}_2. \quad (11)$$

Accordingly, the actual effect of the learned attention on the prediction is represented by the difference between the observed prediction $P(\gamma, X = x_i)$ and its causal intervention one $P(do(\gamma = \bar{\gamma}), X = x_i)$. It is formulated as:

$$P_{effect}^a(x_i) = P(\gamma, X = x_i) - P(do(\gamma = \bar{\gamma}), X = x_i) \quad (12)$$

To this end, the effectiveness of attribute attention can be interpreted as how the attention improves the final prediction compared to the wrong/intervention one. $P_{effect}^a(x_i)$ can be used to evaluate the quality of the learned attribute attention, enabling the attribute features to be more reliable.

3.3 Model Optimization

To optimize MSDN++, each attention sub-net is trained with an attribute-based cross-entropy loss with self-calibration, attribute regression loss, and causal loss. To encourage mutual learning between the two attention sub-nets, we deploy a semantic distillation loss that aligns with each other's class posterior probabilities.

Attribute-Based Cross-Entropy Loss. Considering the associated image and attribute embeddings are projected near their class semantic vector z^c when an attribute is visually present in an image, we take the attribute-based cross-entropy loss with self-calibration (Zhu et al, 2019; Huynh and Elhamifar, 2020a; Xu et al, 2020) (denoted as \mathcal{L}_{ACEC}) to optimize the MSDN++. \mathcal{L}_{ACEC} encourages the image to have the highest compatibility score with its corresponding class semantic vector. Given a batch of n_b training images $\{x_i^s\}_{i=1}^{n_b}$ with their corresponding class semantic vectors z^c , \mathcal{L}_{ACEC} is defined as:

$$\mathcal{L}_{ACEC} = -\frac{1}{n_b} \sum_{i=1}^{n_b} \left[\log \frac{\exp(f(x_i) \times z^c)}{\sum_{\hat{c} \in \mathcal{C}^s} \exp(f(x_i) \times z^{\hat{c}})} - \lambda_{cal} \sum_{c'=1}^{C^u} \log \frac{\exp(f(x_i) \times z^{c'} + \mathbb{I}_{[c' \in \mathcal{C}^u]})}{\sum_{\hat{c} \in \mathcal{C}} \exp(f(x_i) \times z^{\hat{c}} + \mathbb{I}_{[\hat{c} \in \mathcal{C}^u]})} \right], \quad (13)$$

where $f(x_i) = \psi(x_i)$ for AVCA sub-net and $f(x_i) = \Psi(x_i)$ for VACA sub-net, $\mathbb{I}_{[c \in \mathcal{C}^u]}$ is an indicator function (*i.e.*, it is 1 when $c \in \mathcal{C}^u$, otherwise -1), and λ_{cal} is a weight to control the self-calibration term. Intuitively, \mathcal{L}_{ACEC} encourages non-zero probabilities to be assigned to the unseen classes during training, thus MSDN++ produces a large probability for the true unseen class when given the test unseen samples.

Attribute Regression Loss. We employ an attribute regression loss (Xu et al, 2022; Chen et al, 2022a) to optimize MSDN++, which enables \mathcal{M}_1 and \mathcal{M}_2 to map visual/attribute features into semantic spaces close to their corresponding class semantic vectors further. Specifically, we take visual-semantic mapping as a regression problem and minimize the mean square error between the embedded attribute score $f(x_i)$ and the corresponding ground truth attribute score z^c of a batch of n_b images $\{x_i\}_{i=1}^{n_b}$:

$$\mathcal{L}_{AR} = \frac{1}{n_b} \sum_{i=1}^{n_b} \|f(x_i) - z^c\|_2^2. \quad (14)$$

where $f(x_i) = \psi(x_i)$ and $f(x_i) = \Psi(x_i)$ in AVCV and VACA, respectively.

Causal Loss. To enable MSDN++ to learn the intrinsic semantic knowledge for representing reliable features, we deploy the causal loss \mathcal{L}_{causal} based on the causal effect in AVCA (Eq. 6) and VACA (Eq. 12). \mathcal{L}_{causal} can provide a supervision signal to explicitly guide attention learning with



Fig. 3: Part of samples on four challenge datasets, including three fine-grained datasets (*i.e.*, (a) CUB (Welinder et al, 2010), (b) SUN (Patterson and Hays, 2012), and FLO Nilsback and Zisserman (2008)), and one coarse-grained dataset (*i.e.*, AWA2 (Xian et al, 2017)). Each image is sampled from different classes. We find that the images of different classes in fine-grained dataset are very similar and not easy to be distinguished, while the images in the coarse-grained dataset are more easy to be recognized. For example, CUB includes similar bird images, but AWA2 consists of various animal images.

causal associations between visual and attribute representations, formulated as:

$$\begin{aligned} \mathcal{L}_{\text{causal}} &= \frac{1}{n_b} \sum_{i=1}^{n_b} CE(P_{\text{effect}}, y_i), \\ &= -\frac{1}{n_b} \sum_{i=1}^{n_b} \log \frac{\exp(f(x_i) \times z^c)}{\sum_{\hat{c} \in \mathcal{C}^s} \exp(f(x_i) \times z^{\hat{c}})} \\ &\quad - \frac{1}{n_b} \sum_{i=1}^{n_b} \log \frac{\exp(\bar{f}(x_i) \times z^c)}{\sum_{\hat{c} \in \mathcal{C}^s} \exp(\bar{f}(x_i) \times z^{\hat{c}})} \end{aligned} \quad (15)$$

where $P_{\text{effect}} = P_{\text{effect}}^v$ for AVCA and $P_{\text{effect}} = P_{\text{effect}}^a$ for VACA, and CE is the cross-entropy. $f(x_i) = \psi(x_i)$ and $\bar{f}(x_i) = \bar{\psi}(x_i)$ in AVCV, while $f(x_i) = \Psi(x_i)$ and $\bar{f}(x_i) = \bar{\Psi}(x_i)$ in VACA.

Semantic Distillation Loss. We further introduce a semantic distillation loss $\mathcal{L}_{\text{distill}}$, which enables the two mutual attention sub-nets to learn collaboratively and teach each other throughout the training process. $\mathcal{L}_{\text{distill}}$ includes a Jensen-Shannon Divergence (JSD) and an ℓ_2 distance between the predictions of the two sub-nets (*i.e.*, p_1 and p_2). It is formulated as:

$$\begin{aligned} \mathcal{L}_{\text{distill}} &= \frac{1}{n_b} \sum_{i=1}^{n_b} \underbrace{\left[\frac{1}{2} (D_{KL}(p_1(x_i) \| p_2(x_i)) + D_{KL}(p_2(x_i) \| p_1(x_i))) \right]}_{\text{JSD}} \\ &\quad + \underbrace{\|p_1(x_i) - p_2(x_i)\|_2^2}_{\ell_2}, \end{aligned} \quad (16)$$

where

$$D_{KL}(p \| q) = \sum_{c=1}^{C^s} p^c \log \left(\frac{p^c}{q^c} \right). \quad (17)$$

Overall Loss. Finally, the overall loss function of MSDN++ is defined as:

$$\mathcal{L}_{\text{total}} = \mathcal{L}_{\text{ACEC}} + \lambda_{\text{AR}} \mathcal{L}_{\text{AR}} + \lambda_{\text{causal}} \mathcal{L}_{\text{causal}} + \lambda_{\text{distill}} \mathcal{L}_{\text{distill}}, \quad (18)$$

where λ_{AR} , λ_{causal} , and λ_{distill} are weights to control the attribute regression loss, causal loss, and semantic distillation loss, respectively.

3.4 Zero-Shot Prediction

After optimization, We first obtain the embedding features of a test instance x_i in the semantic space w.r.t. the AVCA and VACA sub-nets, *i.e.*, $\psi(x)$ and $\Psi(x)$. Considering the learned semantic knowledge in the two sub-nets are complementary to each other, we fuse their predictions using two combination coefficients (α_1, α_2) to predict the test label of x_i with an explicit calibration, formulated as:

$$c^* = \arg \max_{c \in \mathcal{C}^u / \mathcal{C}} (\alpha_1 \psi(x_i) + \alpha_2 \Psi(x_i))^\top \times z^c + \mathbb{I}_{[c \in \mathcal{C}^u]}. \quad (19)$$

Here, $\mathcal{C}^u / \mathcal{C}$ corresponds to the CZSL/GZSL setting.

4 Experiments

Datasets. To evaluate our method, we conduct experiments on four challenging benchmark datasets, *i.e.*, CUB (Caltech UCSD Birds 200) (Welinder et al, 2010), SUN (SUN Attribute) (Patterson and Hays, 2012), AWA2 (Animals with

Table 1: Results (%) of the state-of-the-art CZSL and GZSL models on CUB, SUN, and AWA2, including generative methods, common space-based methods, and embedding-based methods. The best and second-best results are marked in **Red** and **Blue**, respectively. The symbol “–” indicates no results. The symbol “*” denotes attention-based methods. The symbol † denotes ZSL methods based on large-scale vision-language model.

Methods	CUB				SUN				AWA2			
	CZSL	GZSL			CZSL	GZSL			CZSL	GZSL		
	acc	U	S	H	acc	U	S	H	acc	U	S	H
Generative Methods												
f-CLSWGAN (Xian et al, 2018)	57.3	43.7	57.7	49.7	60.8	42.6	36.6	39.4	68.2	57.9	61.4	59.6
f-VAEGAN-D2 (Xian et al, 2019)	61.0	48.4	60.1	53.6	64.7	45.1	38.0	41.3	71.1	57.6	70.6	63.5
Composer* (Huynh and Elhamifar, 2020b)	69.4	56.4	63.8	59.9	62.6	55.1	22.0	31.4	71.5	62.1	77.3	68.8
GCM-CF (Yue et al, 2021)	–	61.0	59.7	60.3	–	47.9	37.8	42.2	–	60.4	75.1	67.0
FREE (Chen et al, 2021b)	–	55.7	59.9	57.7	–	47.4	37.2	41.7	–	60.4	75.4	67.1
FREE+ESZSL (Cetin et al, 2022)	–	51.6	60.4	55.7	–	48.2	36.5	41.5	–	51.3	78.0	61.8
VS-Boost (Li et al, 2023b)	–	68.0	68.7	68.4	–	49.2	37.4	42.5	–	–	–	–
EGG (Cavazza et al, 2023)	–	58.6	72.3	64.7	–	–	–	–	–	50.2	87.9	63.9
ViFR (Chen et al, 2025)	69.1	57.8	62.7	60.1	65.6	48.8	35.2	40.9	73.7	58.4	81.4	68.0
Common Space Learning												
DeViSE (Frome et al, 2013)	52.0	23.8	53.0	32.8	56.5	16.9	27.4	20.9	54.2	17.1	74.7	27.8
DCN (Liu et al, 2018)	56.2	28.4	60.7	38.7	61.8	25.5	37.0	30.2	65.2	25.5	84.2	39.1
CADA-VAE (Schönfeld et al, 2019)	59.8	51.6	53.5	52.4	61.7	47.2	35.7	40.6	63.0	55.8	75.0	63.9
SGAL (Yu and Lee, 2019)	–	40.9	55.3	47.0	–	35.5	34.4	34.9	–	52.5	86.3	65.3
CLIP† (Radford et al, 2021)	–	55.2	54.8	55.0	–	–	–	–	–	–	–	–
HSVA (Chen et al, 2021c)	62.8	52.7	58.3	55.3	63.8	48.6	39.0	43.3	–	59.3	76.6	66.8
CoOp† (Zhou et al, 2022)	–	49.2	63.8	55.6	–	–	–	–	–	–	–	–
CoOp+SHIP† (Wang et al, 2023)	–	55.3	58.9	57.1	–	–	–	–	–	–	–	–
Embedding-based Methods												
SP-AEN (Chen et al, 2018)	55.4	34.7	70.6	46.6	59.2	24.9	38.6	30.3	58.5	23.3	90.9	37.1
SGMA* (NeurIPS’19) (Zhu et al, 2019)	71.0	36.7	71.3	48.5	–	–	–	–	68.8	37.6	87.1	52.5
AREN* (Xie et al, 2019)	71.8	38.9	78.7	52.1	60.6	19.0	38.8	25.5	67.9	15.6	92.9	26.7
LFGAA* (Liu et al, 2019)	67.6	36.2	80.9	50.0	61.5	18.5	40.0	25.3	68.1	27.0	93.4	41.9
DAZLE* (Huynh and Elhamifar, 2020a)	66.0	56.7	59.6	58.1	59.4	52.3	24.3	33.2	67.9	60.3	75.7	67.1
GNDAN* (Chen et al, 2024b)	75.1	69.2	69.6	69.4	65.3	50.0	34.7	41.0	71.0	60.2	80.8	69.0
TransZero* (Chen et al, 2022a)	76.8	69.3	68.3	68.8	65.6	52.6	33.4	40.8	70.1	61.3	82.3	70.2
APN* (Xu et al, 2022)	75.0	67.4	71.6	69.4	61.5	40.2	35.2	37.5	69.9	61.9	79.4	69.6
ICIS (Christensen et al, 2023)	60.6	45.8	73.7	56.5	51.8	45.2	25.6	32.7	64.6	35.6	93.3	51.6
COND+EGZSL (Chen et al, 2024a)	–	45.2	55.2	49.6	–	–	–	–	–	59.2	80.7	68.3
EG-part-net (Chen et al, 2024c)	–	64.8	66.1	65.4	–	–	–	–	–	64.7	78.7	71.0
MSDN* (Conference Version) (Chen et al, 2022b)	76.1	68.7	67.5	68.1	65.8	52.2	34.2	41.3	70.1	62.0	74.5	67.7
MSDN++* (Ours)	78.5	70.8	70.3	70.6	67.5	51.9	35.4	42.1	73.4	66.5	79.7	72.5

Attributes 2) (Xian et al, 2017) and FLO Nilsback and Zisserman (2008). Among them, CUB, SUN, and FLO are fine-grained datasets, whereas AWA2 is a coarse-grained dataset. Some samples are presented in Fig. 3. Following (Xian et al, 2017), we use the same seen/unseen splits and class semantic embeddings. Specifically, CUB has 11,788 images of 200 bird classes (seen/unseen classes = 150/50) with 312 attributes. SUN consists of 14,340 images of 717 scene classes (seen/unseen classes = 645/72) with 102 attributes. AWA2 has 37,322 images of 50 animal classes (seen/unseen classes = 40/10) with 85 attributes. FLO has 8189 images of 102 flowers classes (seen/unseen classes = 82/20) with 1024 attributes.

Evaluation Protocols. In the CZSL setting, we evaluate the top-1 accuracy on unseen classes, denoted as *acc*. In the GZSL setting, we evaluate the top-1 accuracies both on seen and unseen classes (*i.e.*, *S* and *U*). Furthermore, their harmonic mean (defined as $H = (2 \times S \times U) / (S + U)$) is also used for evaluating the performance in the GZSL setting.

Implementation Details. We take a ResNet101 (He et al, 2016) pre-trained on ImageNet as the network backbone to extract the feature map for each image without fine-tuning. Input images were resized to 448×448 and normalized using ImageNet statistics. The feature maps were extracted from the last convolutional layer, resulting in a fixed spatial dimension of 14×14 (196 regions). This consistent spatial structure was maintained throughout training and intervention. We use the RMSProp optimizer with hyperparameters (momentum = 0.9, weight decay = 0.0001) to optimize our model. We set the learning rate and batch size to 0.0001 and 50, respectively. We take random attention as the causal intervention in causal visual/attribute learning streams for all datasets. Specifically, we generated random attention weights independently for each sample. For the AVCA subnet, random attention matrices of size $[K, 49]$ were sampled from a Uniform(0,1) distribution and then normalized via softmax over the spatial dimension. The same procedure was applied symmetrically to the VACA subnet. These random attentions were used only in the forward pass for causal loss computation and

were detached from the gradient computation, ensuring they did not affect the learning of the actual attention modules. We empirically set the loss weights $\{\lambda_{\text{cal}}, \lambda_{\text{AR}}, \lambda_{\text{causal}}, \lambda_{\text{distill}}\}$ to $\{0.05, 0.03, 0.3, 0.001\}$, $\{0.0001, 0.01, 0.0005, 0.05\}$, and $\{0.4, 0.06, 0.1, 0.01\}$ for CUB, SUN, and AWA2, respectively. We set the combination coefficient (α_1, α_2) to $(0.8, 0.2)$, $(0.7, 0.3)$, $(0.8, 0.2)$ for CUB, SUN, and AWA2, respectively.

Table 2: Results (%) of the state-of-the-art GZSL models on FLO.

Methods	FLO		
	U	S	H
f-CLSWGAN (Xian et al, 2018)	59.3	74.2	65.9
f-VAEGAN-D2 (Xian et al, 2019)	56.8	74.9	64.6
TF-VAEGAN (Narayan et al, 2020)	62.5	84.1	71.7
EG-part-net (Chen et al, 2024c)	61.5	81.4	70.1
MSDN(Conference Version) (Chen et al, 2022b)	62.2	81.0	70.3
MSDN++ (Ours)	69.2	80.7	74.5

4.1 Comparison with State-of-the-Arts

Our MSDN++ is an embedding-based method with inductive manner. To demonstrate the effectiveness and advantages of our MSDN++, we compare it with other state-of-the-art methods both in CZSL and GZSL settings, including generative methods (*e.g.*, f-CLSWGAN (Xian et al, 2018), f-VAEGAN (Xian et al, 2019), Composer (Huynh and Elhamifar, 2020b), E-PGN (Yu et al, 2020), TF-VAEGAN (Narayan et al, 2020), IZF (Shen et al, 2020), SDGZSL (Chen et al, 2021d), GCM-CF (Yue et al, 2021), FREE (Chen et al, 2021b), FREE+ESZSL (Cetin et al, 2022), VS-Boost (Li et al, 2023b), EGG (Cavazza et al, 2023), and ViFR (Chen et al, 2025)), common space learning methods (*e.g.*, DeViSE (Frome et al, 2013), DCN (Liu et al, 2018), CADA-VAE (Schönfeld et al, 2019), SGAL (Yu and Lee, 2019), and HSVA (Chen et al, 2021c), CLIP (Radford et al, 2021), CoOp (Zhou et al, 2022), CoOp+SHIP (Wang et al, 2023)), and embedding-based methods (*e.g.*, SP-AEN (Chen et al, 2018), SGMA, AREN (Xie et al, 2019), LFGAA (Liu et al, 2019), DAZLE (Huynh and Elhamifar, 2020a), GNDAN (Chen et al, 2024b), TransZero (Chen et al, 2022a), APN (Xu et al, 2022), ICIS (Christensen et al, 2023), EG-part-net (Chen et al, 2024c), COND+EGZSL (Chen et al, 2024a)). Notably, the large-scale visual-language model based ZSL methods (Radford et al, 2021; Zhou et al, 2022; Wang et al, 2023) can be grouped into common space learning methods intrinsically. Different to classical common space learning methods (Frome et al, 2013; Schönfeld et al, 2019; Chen et al, 2021c) that uses small datasets for learning a joint space of visual and semantic representations with semantic attributes, the large-scale visual-language model

based ZSL methods learns the joint space with large-scale data and label prompt.

Conventional Zero-Shot Learning. We first compare our MSDN++ with the state-of-the-art methods in the CZSL setting. Table 1 shows the results of CZSL on various datasets. Compared to all strong baselines, including embedding-based methods, generative methods, and common space learning methods, our MSDN++ performs the best results of 78.5%, 67.5%, and second-best results of 73.4% on CUB, SUN, and AWA2, respectively. This indicates that MSDN++ discovers the intrinsic semantic knowledge for effective knowledge transfer from seen classes to unseen ones. Furthermore, our MSDN++ achieves significant performance gains by 2.4%, 1.7%, and 3.3% on CUB, SUN, and AWA2, respectively, over the MSDN (conference version). This should be thanks to the causal visual/attribute leanings that guide MSDN++ to learn causal vision-attribute associations for representing reliable features with good generalization.

Generalized Zero-Shot Learning. We take MSDN++ to compare with the state-of-the-art methods in the GZSL setting further. Results are shown in Table 1. We can find:

- i)* The most state-of-the-art methods achieve good results on seen classes but fail on unseen classes on CUB and AWA2. For example, AREN (Xie et al, 2019) and LFGAA (Liu et al, 2019) get the accuracies on unseen/seen classes are 38.9%/78.7% (15.6%/92.9%) and 36.2%/80.9% (27.0%/93.4%) on CUB (AWA2), respectively. Because they simply utilize unidirectional attention in a weakly supervised manner to learn the spurious and limited latent semantic representations, which fails to effectively discover the intrinsic semantic knowledge for knowledge transfer from seen to unseen classes. In contrast, our MSDN++ employs a mutually causal semantic distillation network to learn intrinsic and more efficient semantic knowledge, which enables the model to generalize well to unseen classes with high seen and unseen accuracies. Accordingly, MSDN++ obtains good results of harmonic mean, *i.e.*, 70.6%, 42.1%, and 72.5% on CUB, SUN, and AWA2, respectively.
- ii)* Compared to the large-scale vision-language model based ZSL methods (*e.g.*, CLIP (Radford et al, 2021), CoOp (Zhou et al, 2022), CoOp+SHIP (Wang et al, 2023)), our MSDN++ obtains significant performances gains of $H = 13.5\%$ at least on CUB. This demonstrates the superiority and potential of our MSDN++ for ZSL. Because the large-scale vision-language based ZSL methods are limited by the domain-specific knowledge, which has a large bias with the large-scale vision-text pairs.
- iii)* GCM-CF (Yue et al, 2021) is the first method that applied causal inference to the ZSL task. It introduces a causal generation to guide the generative methods to synthesize balanced visual features for unseen classes. Differently, we design causal attention learning to enable the embedding-based methods to learn intrinsic and more sufficient seman-

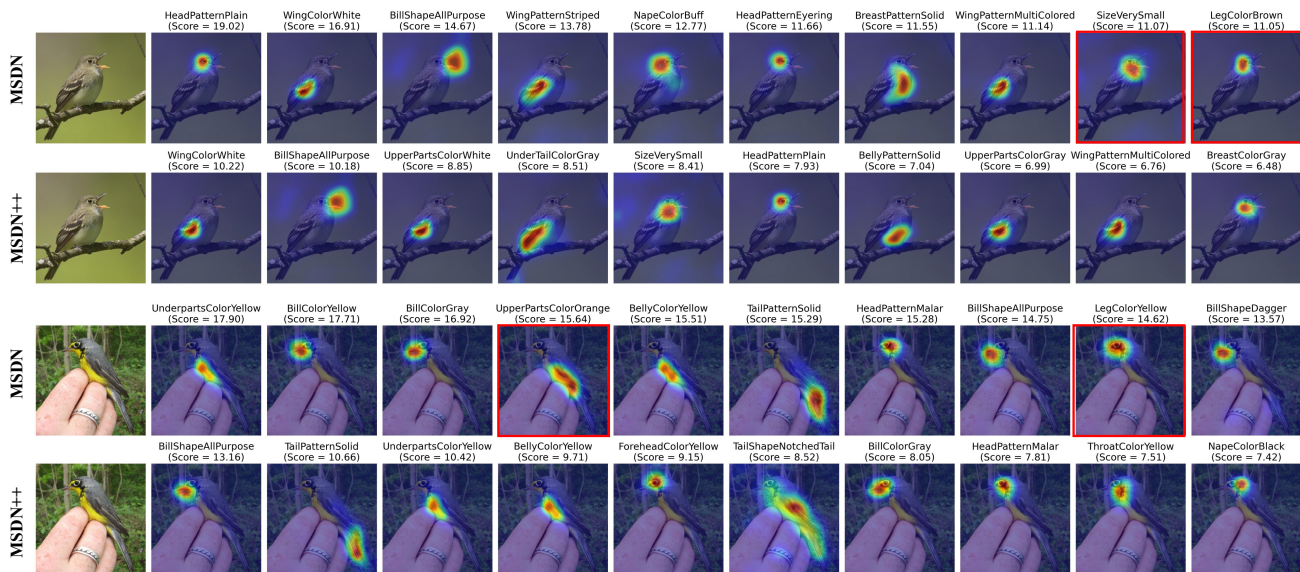


Fig. 4: Visualization of attention maps learned by the first sub-nets of MSDN (Chen et al, 2022b) and MSDN++ on CUB. We show the top-10 attention maps focused by models. The red boxes indicate MSDN learns the wrong attention maps that are irrelevant to the corresponding attributes.

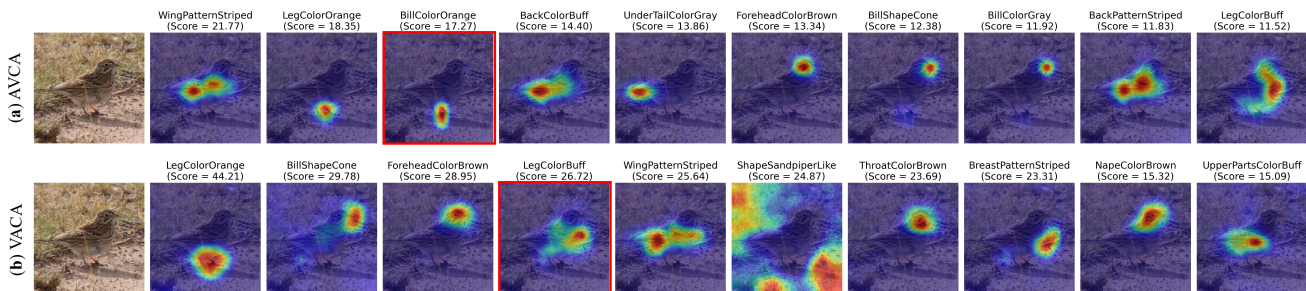


Fig. 5: Visualization of attention maps for the two mutual attention sub-nets (i.e, MSDN++(AVCA) and MSDN++(VACA)). Results show that our AVCA and VACA subnets can overall learn the accurate visual localizations, but they also learn few of failure cases.

tic knowledge for knowledge transfer from seen to unseen classes. Our MSDN++ achieves significant improvements of harmonic mean by 10.3% and 5.5% on CUB and AWA2, respectively.

iv) MSDN++ performs poorer than the generative methods in the GZSL setting because per class only contains 16 training images on SUN, which heavily limits the ZSL models. As such, the data augmentation is very effective for improving the performance of SUN, e.g., the generative methods VS-Boost (Li et al, 2023b), HSVa (Chen et al, 2021c). Thus, most of the generative methods perform better than the embedding-based methods on SUN.

Additionally, we also conduct experiments on FLO dataset Nilsback and Zisserman (2008), results are shown in Table 2. Results show that our MSDN++ achieves the best result of $H = 74.5\%$ on FLO. Compared to our conference version (MSDN Chen et al (2022b)), our MSDN++ obtains

Table 3: Ablation studies for different components of MSDN++. The *baseline* is the visual feature extracted from CNN backbone with a global average pooling and then mapped into semantic embedding for ZSL.

Method	CUB				AWA2			
	acc	U	S	H	acc	U	S	H
baseline	57.4	44.2	55.2	49.1	54.8	30.3	30.7	30.5
baseline w/ \mathcal{L}_{AR}	58.5	46.5	54.6	50.2	56.9	20.6	89.7	33.5
MSDN++(AVCA) w/o $\mathcal{L}_{distill}$	76.2	68.7	69.1	68.9	71.9	65.5	76.8	70.7
MSDN++(VACA) w/o $\mathcal{L}_{distill}$	68.4	57.5	65.6	61.3	68.0	56.5	74.6	64.3
MSDN++(AVCA) w/ $\mathcal{L}_{distill}$	77.7	69.6	70.0	69.8	73.0	66.4	79.3	72.3
MSDN++(VACA) w/ $\mathcal{L}_{distill}$	70.8	59.9	65.3	62.5	70.3	60.3	76.3	67.3
MSDN++ w/o AVCA (\mathcal{L}_{causal})	77.5	67.8	71.5	69.6	72.9	66.5	77.9	71.8
MSDN++ w/o VACA (\mathcal{L}_{causal})	77.9	70.6	70.2	70.4	73.3	66.9	78.4	72.2
MSDN++ w/o \mathcal{L}_{causal}	77.0	69.6	69.2	69.4	72.7	66.1	78.4	71.7
MSDN++	78.5	70.8	70.3	70.6	73.4	66.5	79.7	72.5

performance gain of H with 4.2%. These demonstrate the improvements of MSDN++ using causal attention.

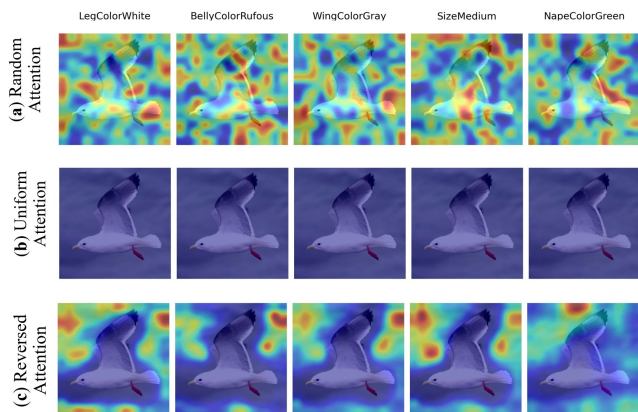


Fig. 6: The attention maps of various causal interventions, including (a) random attention, (b) uniform attention, and (c) reversed attention.

4.2 Ablation Studies

We conduct ablation studies to evaluate the effectiveness of various components of MSDN++, including the AVCA attention sub-net (denoted as MSDN(AVCA) w/o $\mathcal{L}_{\text{distill}}$), VACA attention sub-net (denoted as MSDN(VACA) w/o $\mathcal{L}_{\text{distill}}$), semantic distillation learning (*i.e.*, MSDN(VACA) w/ $\mathcal{L}_{\text{distill}}$, MSDN(AVCA) w/ $\mathcal{L}_{\text{distill}}$), causal visual learning (MSDN++ w/o AVCA($\mathcal{L}_{\text{causal}}$)), causal attribute learning (MSDN++ w/o VACA($\mathcal{L}_{\text{causal}}$)), and causal learning (*i.e.*, MSDN w/o $\mathcal{L}_{\text{causal}}$). Results are shown in Table 3. Compared to the baseline, MSDN++ only employs the single attention sub-net without semantic distillation obtaining significant performance gains. For example, MSDN(AVCA) w/o $\mathcal{L}_{\text{distill}}$ achieves the gains of *acc/H* by 18.8%/19.8% and 17.1%/40.2% on CUB and AWA2, respectively; MSDN++(VACA) w/o $\mathcal{L}_{\text{distill}}$ achieves the *acc/H* improvements of 11.0%/12.2% and 13.2%/33.8% on CUB and AWA2, respectively. Because MSDN++ discovers the intrinsic semantic knowledge using causal learning and visual/attribute-based attribute/visual learning to refine the visual features for effective knowledge transfer. When MSDN++ adopts semantic distillation loss to conduct collaborative learning for knowledge distillation, its results can be further improved, *e.g.*, MSDN(VACA) improves the *acc/H* by 2.4%/1.2% and 2.3%/3.0% on CUB and AWA2, respectively. The causal attribute/visual learning consistently improve the performance of MSDN++ by guiding the model to learn causal vision-attribute associations for representing reliable features. Moreover, the two causal learning can further improve MSDN++ cooperatively. We also find that the model significantly overfits to seen classes without our mutual semantic distillation and causal learning. Our full model ensembles the complementary embeddings learned by the two mutual causal attention sub-nets to rep-

Table 4: Effects of various causal interventions on CUB, *i.e.*, (a) Random Attention, (b) Uniform Attention, (c) Reversed Attention, and (d) Random Attention+Reversed Attention.

Method	CUB			
	acc	U	S	H
MSDN (Chen et al, 2022b)	76.1	68.7	67.5	68.1
MSDN++ w/ (a)	78.5	70.8	70.3	70.6
MSDN++ w/ (b)	78.4	70.8	70.0	70.4
MSDN++ w/ (c)	78.0	71.0	69.9	70.5
MSDN++ w/ (d)	78.5	71.8	69.5	70.6

resent sufficient semantic knowledge, resulting in further performance gains for MSDN++.

4.3 Qualitative Results

Visualization of Attention Maps. To intuitively show the effectiveness of our MSDN++ for learning more intrinsic semantic knowledge than MSDN (Chen et al, 2022b), we visualize the top-10 attention maps learned by the two methods. As shown in Fig. 4, although MSDN can localize some attributes in the image correctly for semantic knowledge representations, a few of the attributes are localized wrongly. For example, the MSDN localizes the attribute “leg color brown” of *Acadian Flycatcher* on the head in the image. This is because MSDN learns the wrong associations between visual and attribute features for representing spurious semantic knowledge. In contrast, our MSDN++ learns the important attribute localization accurately for intrinsic semantic knowledge representations using causal attribute/visual learning, which encourages MSDN++ to discover the causal vision-attribute associations for representing reliable features. As shown in Fig. 5, the two sub-nets of MSDN++ can similarly learn the most important semantic representation, which is beneficial from mutual learning for semantic distillation. Furthermore, the two attention sub-nets also learn the complementary attribute feature localization for each other. As such, our MSDN++ achieves significant performance gains over MSDN.

Although our AVCA and VACA subsets can overall learn the accurate visual localizations, they also learn few of failure cases. For example, the attribute “Bill Color Orange” and the attribute “Leg Color Buff” are wrongly localized by AVCA and VACA, respectively. This may be caused by the semantic ambiguity, which denotes that the same attribute may be represented as various visual appearances. We believe this is an open challenge for future works.

t-SNE Visualizations. As shown in Fig. 7, we also present the t-SNE visualization (Maaten and Hinton, 2008) of visual features for seen and unseen classes on CUB, learned by the baseline, MSDN (Chen et al, 2022b), and MSDN++. Compared to the baseline, our models learn the intrinsic semantic

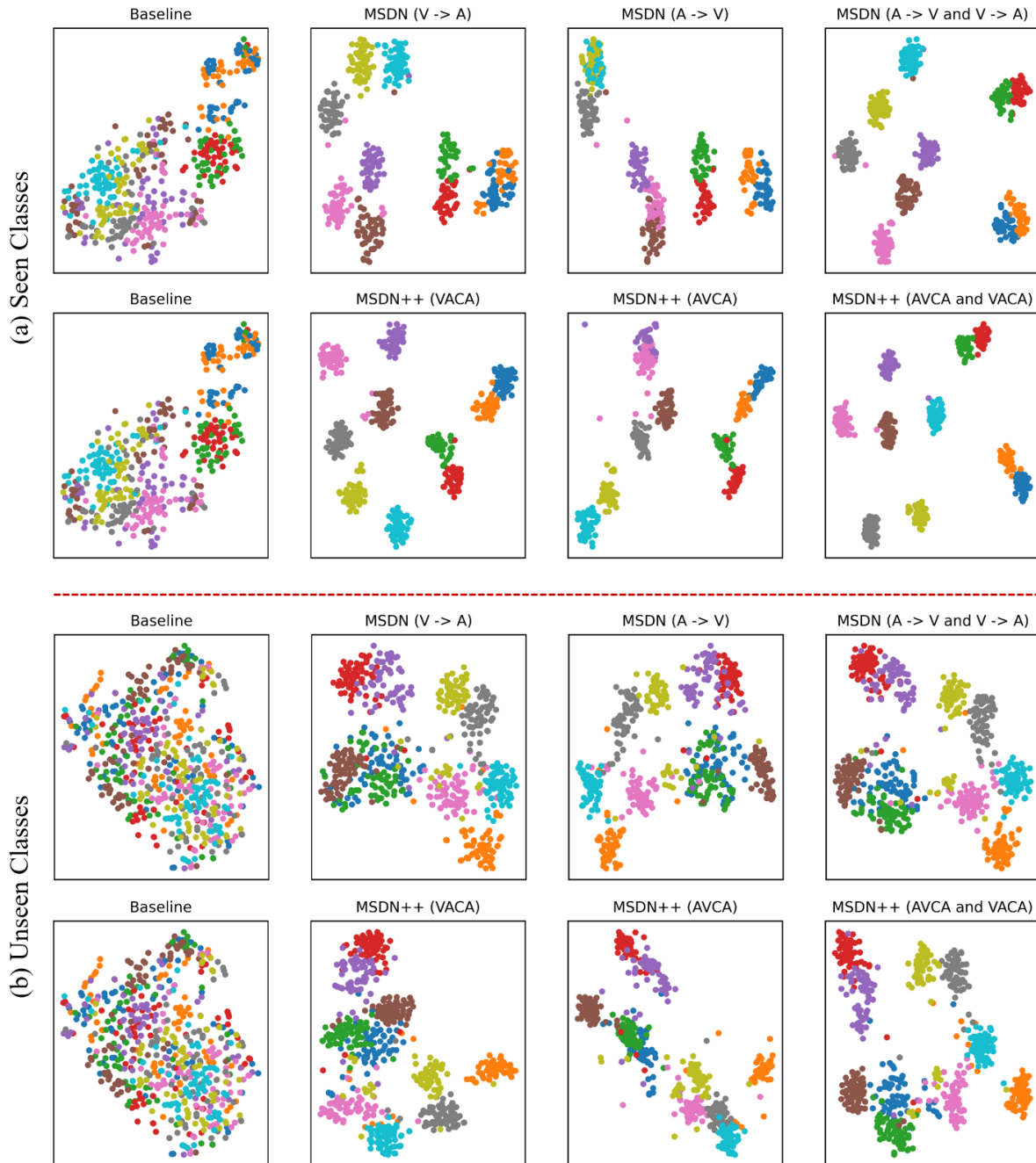


Fig. 7: t-SNE visualizations of visual features for (a) seen classes and (b) unseen classes, learned by the baseline, MSDN (Chen et al, 2022b), and MSDN++. The 10 colors denote 10 different seen/unseen classes randomly selected from CUB. Results show that our MSDN++ learn the intrinsic semantic representations both in seen and unseen classes compared to the baseline. Meanwhile, the each subnet of MSDN++ consistently enhances the intra-class compactness and inter-classes separability for MSDN.

representations both in seen and unseen classes. For each subnet, MSDN++ consistently enhances the intra-classes compactness and inter-classes separability for MSDN, and thus the fused features are refined further. This should be thanks to our causal visual/attributes learning in the AVCA/VACA subnets, which encourage MSDN++ to learn causal vision-

attribute associations for representing reliable features with good generalization. As such, our MSDN++ achieves significant improvement over MSDN and baseline.

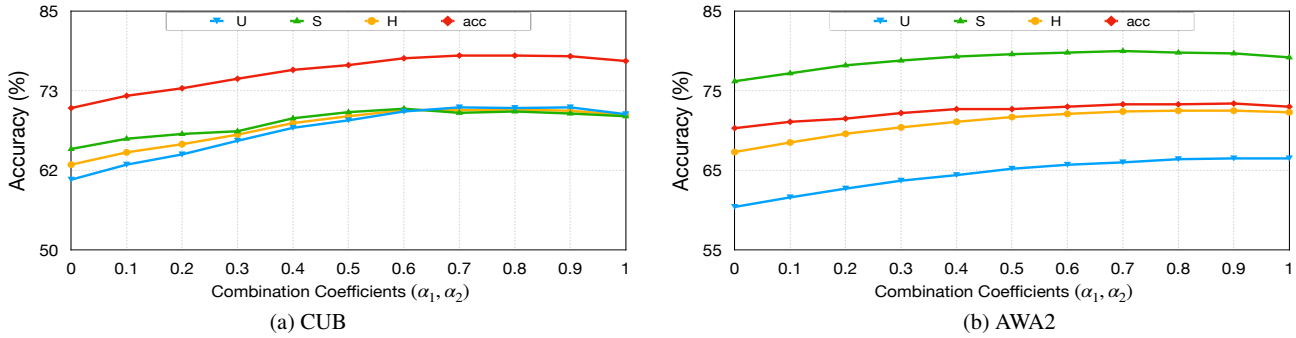


Fig. 8: The effectiveness of the combination coefficients (α_1, α_2) between the AVCA and VACA sub-nets. Results show that MSDN++ performs poorly when α_1/α_2 is set small, and its performances drop down when α_1/α_2 is set too large. Because the attribute-based visual features and visual-based attribute features are complementary for discriminative semantic embedding representations.

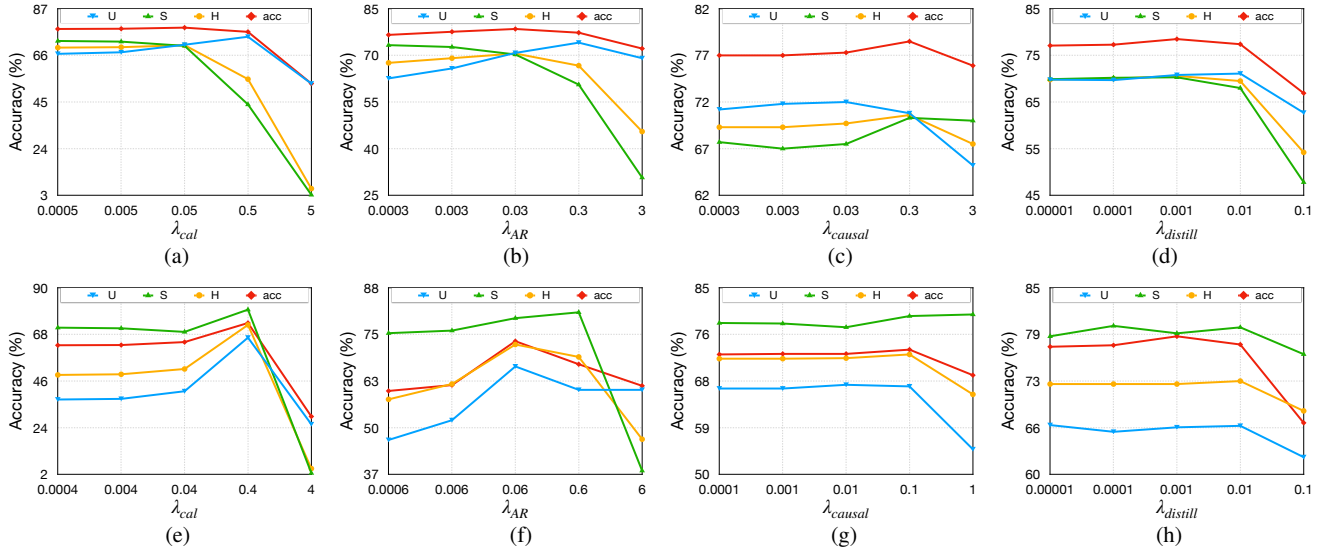


Fig. 9: The effects of λ_{cal} , λ_{AR} , λ_{causal} , and $\lambda_{distill}$ on CUB (top-row) and AWA2 (bottom-row). Results show that MSDN++ is robust when the loss weights are set to small and the performance will drop rapidly when loss weights are set to too large. Because the large loss weights will hamper the balance of various losses.

4.4 Effects of Various Causal Intervention

We analyze three different strategies to conduct a causal intervention, including random attention, uniform attention and reversed attention, which will generate various causal attention maps as shown in Fig. 6. Results show that the causal attention maps focus on the wrong visual regions, which are not relevant to their corresponding attributes. This causal can measure the effectiveness of our attribute-based visual learning and visual-based attribute learning and enable them to learn the intrinsic semantic knowledge between visual and attribute features with causality. The results in Table 4 show that the various causal attentions consistently improve the performance of MSDN. Because our causal

attention provides a significant signal to supervise MSDN++. Furthermore, we find that all the causal interventions get similar performance gains, which indicates our causal visual/attribute learning is robust for improving the causality of features.

4.5 Hyperparameter Analysis

Effects of Combination Coefficients. we provide experiments to determine the effectiveness of the combination coefficients (α_1, α_2) between AVCA and VACA sub-nets. As shown in Fig. 8, MSDN++ performs poorly when α_1/α_2 is set small, because the AVCA is the main sub-net to support the final classification of MSDN++. Since the attribute-

based visual features and visual-based attribute features are complementary for discriminative semantic embedding representations, the performances of MSDN++ drop down when α_1/α_2 is set too large (e.g., $(\alpha_1, \alpha_2) = (0.9, 0.1)$). According to Fig. 8, we set (α_1, α_2) to be (0.8,0.2) for CUB and AWA2 based on the performances of H and acc . Notably, $(\alpha_1, \alpha_2) = (1.0, 0.0)$ and $(\alpha_1, \alpha_2) = (0.0, 1.0)$ denotes the MSDN++ without information fusion from AVCA and VACA during inference.

Effects of Loss Weights. We empirically study how to set the related loss weights of MSDN++: λ_{cal} , λ_{AR} , λ_{causal} , and $\lambda_{distill}$, which control the self-calibration term, attribute regression loss, causal loss, and semantic distillation loss, respectively. Results are shown in Fig. 9. Results show that MSDN++ is robust when the loss weights are set to small and the performance will drop rapidly when loss weights are set to too large. Because the large loss weights will hamper the balance of various losses. According to the results in Fig. 9, we set the loss weights $\{\lambda_{cal}, \lambda_{AR}, \lambda_{causal}, \lambda_{distill}\}$ to $\{0.05, 0.03, 0.3, 0.001\}$ and $\{0.4, 0.06, 0.1, 0.01\}$ for CUB and AWA2, respectively. Notably, the loss weights $\{\lambda_{cal}, \lambda_{AR}, \lambda_{causal}, \lambda_{distill}\}$ are to $\{0.0001, 0.01, 0.0005, 0.05\}$ for SUN. Furthermore, although the performance curve somehow unstale with the variant values for the hyper-parameters, MSDN++ performs consistently on various datasets when using same hyper-parameters. This means that our MSDN++ is robust on various datasets. Accordingly, our method can be easily applied into new domains.

5 Conclusion

This paper introduces a mutually causal distillation network for ZSL, termed MSDN++, which consists of an AVCA and a VACA sub-nets. AVCA learns the attribute-based visual features with attribute-based/ causal visual learnings, while VACA learns the visual-based attribute features via visual-based/ causal attribute learnings. The causal attentions encourage the two sub-nets to discover causal vision-attribute associations for representing reliable features with good generalization. Furthermore, we further introduce a semantic distillation loss, which promotes the two sub-nets to learn collaboratively and teach each other. Finally, we fuse the complementary features of the two sub-nets to make full use of all important knowledge during inference. As such, MSDN++ effectively explores the intrinsic and more sufficient semantic knowledge for desirable knowledge transfer in ZSL. The quantitative and qualitative results on three popular benchmarks (i.e., CUB, SUN, and AWA2) demonstrate the superiority and potential of our MSDN++.

Data Availability Statements

The data used in this manuscript includes three benchmark datasets, i.e., CUB,¹ SUN,² and AWA2,³ which are publicly opened benchmarks.

References

- Akata Z, Perronnin F, Harchaoui Z, Schmid C (2016) Label-embedding for image classification. TPAMI 38:1425–1438
- Arora G, Verma V, Mishra A, Rai P (2018) Generalized zero-shot learning via synthesized examples. In: CVPR, pp 4281–4289
- Bai X, Wang H, Ma L, Xu Y, Gan J, Fan Z, Yang F, Ma K, Yang J, Bai S, Shu C, Zou X, Huang R, Zhang C, Liu X, Tu D, Xu C, Zhang W, Wang XL, Chen A, Zeng Y, Yang D, Wang MW, Holalkere NS, Halin NJ, Kamel IR, Wu J, Peng X, Wang X, Shao J, Mongkolwat P, Zhang J, Liu W, Roberts M, Teng Z, Beer L, Sanchez LE, Sala E, Rubin D, Weller A, Lasenby J, Zheng C, Wang J, Li Z, Schönlieb CB, Xia T (2021) Advancing covid-19 diagnosis with privacy-preserving collaboration in artificial intelligence. Nature Machine Intelligence
- Cavazza J, Murino V, Bue AD (2023) No adversaries to zero-shot learning: Distilling an ensemble of gaussian feature generators. IEEE Transactions on Pattern Analysis and Machine Intelligence 45:12167–12178
- Cetin S, Baran OB, Cinbis RG (2022) Closed-form sample probing for learning generative models in zero-shot learning. In: ICLR
- Chen D, Zhang H, Shen Y, Long Y, Shao L (2024a) Evolutionary generalized zero-shot learning. In: IJCAI
- Chen G, Li J, Lu J, Zhou J (2021a) Human trajectory prediction via counterfactual analysis. In: ICCV, pp 9804–9813
- Chen L, Zhang H, Xiao J, Liu W, Chang S (2018) Zero-shot visual recognition using semantics-preserving adversarial embedding networks. In: CVPR, pp 1043–1052
- Chen S, Wang W, Xia B, Peng Q, You X, Zheng F, Shao L (2021b) Free: Feature refinement for generalized zero-shot learning. In: ICCV
- Chen S, Xie GS, Yang Liu Y, Peng Q, Sun B, Li H, You X, Shao L (2021c) Hsva: Hierarchical semantic-visual adaptation for zero-shot learning. In: NeurIPS
- Chen S, Hong Z, Liu Y, Xie G, Sun B, Li H, Peng Q, Lu K, You X (2022a) Transzero: Attribute-guided transformer for zero-shot learning. In: AAAI

¹ https://www.vision.caltech.edu/datasets/cub_200_2011/

² <https://cs.brown.edu/~gmpatter/sunattributes.html>

³ <https://cvml.ist.ac.at/AWA2/>

- Chen S, Hong Z, Xie G, Wang W, Peng Q, Wang K, Jun Zhao J, You X (2022b) Msdn: Mutually semantic distillation network for zero-shot learning. In: CVPR, pp 7602–7611
- Chen S, Hong ZQ, Xie G, Zhao J, Li H, You X, Yan S, Shao L (2023a) Transzero++: Cross attribute-guided transformer for zero-shot learning. *IEEE Transactions on Pattern Analysis and Machine Intelligence* 45(11):12844–12861
- Chen S, Hou WQ, Hong Z, Ding X, Song Y, You X, Liu T, Zhang K (2023b) Evolving semantic prototype improves generative zero-shot learning. In: ICML
- Chen S, Hong Z, Xie G, Peng Q, You X, Ding W, Shao L (2024b) Gndan: Graph navigated dual attention network for zero-shot learning. *IEEE Transactions on Neural Networks and Learning Systems* 35(4):4516–4529
- Chen S, Hong Z, You X, Shao L (2025) Semantics-conditioned generative zero-shot learning via feature refinement. *International of Computer Vision* 133(7):4504–4521
- Chen X, Deng X, Lan Y, Long Y, Weng J, Liu Z, Tian Q (2024c) Explanatory object part aggregation for zero-shot learning. *IEEE Transactions on Pattern Analysis and Machine Intelligence* 46(2):851–868
- Chen Z, Luo Y, Qiu R, Wang S, Huang Z, Li J, Zhang Z (2021d) Semantics disentangling for generalized zero-shot learning. In: ICCV
- Chou YY, Lin HT, Liu TL (2021) Adaptive and generative zero-shot learning. In: ICLR
- Christensen A, Mancini M, Koepke AS, Winther O, Akata Z (2023) Image-free classifier injection for zero-shot classification. In: ICCV
- Collins RT, Lipton AJ, Kanade T, Fujiyoshi H, Duggins D, Tsin Y, Tolliver D, Enomoto N, Hasegawa O, Burt PJ, Wixson LE (2000) A system for video surveillance and monitoring. Carnegie Mellon University Technical Report, CMU-RI-TR-00-12
- Frappier M (2018) The book of why: The new science of cause and effect. *Science* 361:855 – 855
- Frome A, Corrado GS, Shlens J, Bengio S, Dean J, Ranzato M, Mikolov T (2013) Devise: A deep visual-semantic embedding model. In: NeurIPS
- Fu Y, Timothy MH, Xiang-tao, Gong S (2015) Transductive multi-view zero-shot learning. *TPAMI* pp 2332–2345
- Han Z, Fu Z, Yang J (2020) Learning the redundancy-free features for generalized zero-shot object recognition. In: CVPR, pp 12862–12871
- Han Z, Fu Z, Chen S, Yang J (2021) Contrastive embedding for generalized zero-shot learning. In: CVPR
- He K, Zhang X, Ren S, Sun J (2016) Deep residual learning for image recognition. In: CVPR, pp 770–778
- Hinton GE, Vinyals O, Dean J (2015) Distilling the knowledge in a neural network. *arXiv preprint arXiv:150302531*
- Hu Y, Yang J, Chen L, Li K, Sima C, Zhu X, Chai S, Du S, Lin T, Wang W, Lu L, Jia X, Liu Q, Dai J, Qiao Y, Li H (2023) Planning-oriented autonomous driving. In: CVPR, pp 17853–17862
- Huynh D, Elhamifar E (2020a) Fine-grained generalized zero-shot learning via dense attribute-based attention. In: CVPR, pp 4482–4492
- Huynh DT, Elhamifar E (2020b) Compositional zero-shot learning via fine-grained dense feature composition. In: NeurIPS
- Kallus N, Zhou A (2018) Confounding-robust policy improvement. In: NeurIPS, p 9269–9279
- Keshari R, Singh R, Vatsa M (2020) Generalized zero-shot learning via over-complete distribution. In: CVPR, pp 13297–13305
- Lampert CH, Nickisch H, Harmeling S (2009) Learning to detect unseen object classes by between-class attribute transfer. In: CVPR, pp 951–958
- Lampert CH, Nickisch H, Harmeling S (2014) Attribute-based classification for zero-shot visual object categorization. *TPAMI* 36:453–465
- Larochelle H, Erhan D, Bengio Y (2008) Zero-data learning of new tasks. In: AAAI, pp 646–651
- Li J, Jing M, Lu K, Ding Z, Zhu L, Huang Z (2019a) Leveraging the invariant side of generative zero-shot learning. In: CVPR, pp 7394–7403
- Li J, Zhang Y, Qiang W, Si L, Jiao C, Hu X, Zheng C, Sun F (2023a) Disentangle and remerge: Interventional knowledge distillation for few-shot object detection from a conditional causal perspective. In: AAAI, pp 1323–1333
- Li K, Min MR, Fu Y (2019b) Rethinking zero-shot learning: A conditional visual classification perspective. In: ICCV, pp 3582–3591
- Li X, Zhang Y, Bian S, Qu Y, Xie Y, Shi Z, Fan J (2023b) Vs-boost: Boosting visual-semantic association for generalized zero-shot learning. In: IJCAI
- Li X, Sun S, Feng R (2024) Causal representation learning via counterfactual intervention. In: AAAI
- Li Y, Zhang J, Zhang J, Huang K (2018) Discriminative learning of latent features for zero-shot recognition. In: CVPR, pp 7463–7471
- Liu S, Long M, Wang J, Jordan MI (2018) Generalized zero-shot learning with deep calibration network. In: NeurIPS
- Liu Y, Guo J, Cai D, He X (2019) Attribute attention for semantic disambiguation in zero-shot learning. In: ICCV, pp 6697–6706
- Liu Y, Zhou L, Bai X, Huang Y, Gu L, Zhou J, Harada T (2021) Goal-oriented gaze estimation for zero-shot learning. In: CVPR
- Lv F, Liang J, Li S, Zang B, Liu CH, Wang Z, Liu D (2022) Causality inspired representation learning for domain generalization. In: CVPR, pp 8036–8046
- Maaten LVD, Hinton GE (2008) Visualizing data using t-sne. *JMLR* 9:2579–2605

- Min S, Yao H, Xie H, Wang C, Zha Z, Zhang Y (2020) Domain-aware visual bias eliminating for generalized zero-shot learning. In: CVPR, pp 12661–12670
- Narayan S, Gupta A, Khan F, Snoek CGM, Shao L (2020) Latent embedding feedback and discriminative features for zero-shot classification. In: ECCV
- Nilsback ME, Zisserman A (2008) Automated flower classification over a large number of classes. In: ICVGIP, pp 722–729
- Palatucci M, Pomerleau D, Hinton GE, Mitchell TM (2009) Zero-shot learning with semantic output codes. In: NeurIPS, pp 1410–1418
- Parisotto E, Ba J, Salakhutdinov R (2016) Actor-mimic: Deep multitask and transfer reinforcement learning. In: ICLR
- Patterson G, Hays J (2012) Sun attribute database: Discovering, annotating, and recognizing scene attributes. In: CVPR, pp 2751–2758
- Pearl J (2009) Causality, 2nd edn. Cambridge University Press
- Pearl J, Glymour M, Jewell NP (2016) Causal inference in statistics: A primer. John Wiley & Son
- Pennington J, Socher R, Manning CD (2014) Glove: Global vectors for word representation. In: EMNLP
- Pourpanah F, Abdar M, Luo Y, Zhou X, Wang R, Lim CP, Wang X (2020) A review of generalized zero-shot learning methods. IEEE Transactions on Pattern Analysis and Machine Intelligence 45:4051–4070
- Radford A, Kim JW, Hallacy C, Ramesh A, Goh G, Agarwal S, Sastry G, Askell A, Mishkin P, Clark J, Krueger G, Sutskever I (2021) Learning transferable visual models from natural language supervision. In: ICML
- Rao Y, Chen G, Lu J, Zhou J (2021) Counterfactual attention learning for fine-grained visual categorization and re-identification. In: ICCV, pp 1005–1014
- Romera-Paredes B, Torr PHS (2015) An embarrassingly simple approach to zero-shot learning. In: ICML
- Romero A, Ballas N, Kahou SE, Chassang A, Gatta C, Bengio Y (2015) Fitnets: Hints for thin deep nets. In: ICLR
- Schönfeld E, Ebrahimi S, Sinha S, Darrell T, Akata Z (2019) Generalized zero- and few-shot learning via aligned variational autoencoders. In: CVPR, pp 8239–8247
- Shen Y, Qin J, Huang L (2020) Invertible zero-shot recognition flows. In: ECCV
- Song J, Shen C, Yang Y, Liu Y, Song M (2018) Transductive unbiased embedding for zero-shot learning. CVPR pp 1024–1033
- Tang K, Niu Y, Huang J, Shi J, Zhang H (2020) Unbiased scene graph generation from biased training. In: CVPR, pp 3713–3722
- Tsai YHH, Huang LK, Salakhutdinov R (2017) Learning robust visual-semantic embeddings. In: ICCV, pp 3591–3600
- Vyas MR, Venkateswara H, Panchanathan S (2020) Leveraging seen and unseen semantic relationships for generative zero-shot learning. In: ECCV
- Wang K, Peng X, Yang J, Lu S, Qiao Y (2020a) Suppressing uncertainties for large-scale facial expression recognition. In: CVPR, pp 6897–6906
- Wang K, Peng X, Yang J, Meng D, Qiao Y (2020b) Region attention networks for pose and occlusion robust facial expression recognition. IEEE Transactions on Image Processing 29:4057–4069
- Wang T, Zhou C, Sun Q, Zhang H (2021a) Causal attention for unbiased visual recognition. In: ICCV, pp 3071–3080
- Wang Z, Gou Y, Li J, Zhang Y, Yang Y (2021b) Region semantically aligned network for zero-shot learning. In: CIKM
- Wang Z, Liang J, He R, Xu N, Wang Z, Tan TP (2023) Improving zero-shot generalization for clip with synthesized prompts. In: ICCV
- Welinder P, Branson S, Mita T, Wah C, Schroff F, Belongie SJ, Perona P (2010) Caltech-ucsd birds 200. Technical Report CNS-TR-2010-001, Caltech,
- Wood-Doughty Z, Shpitser I, Dredze M (2018) Challenges of using text classifiers for causal inference. In: EMNLP, pp 4586–4598
- Xian Y, Schiele B, Akata Z (2017) Zero-shot learning — the good, the bad and the ugly. In: CVPR, pp 3077–3086
- Xian Y, Lorenz T, Schiele B, Akata Z (2018) Feature generating networks for zero-shot learning. In: CVPR, pp 5542–5551
- Xian Y, Sharma S, Schiele B, Akata Z (2019) F-vaegan-d2: A feature generating framework for any-shot learning. In: CVPR, pp 10267–10276
- Xie GS, Liu L, Jin X, Zhu F, Zhang Z, Qin J, Yao Y, Shao L (2019) Attentive region embedding network for zero-shot learning. In: CVPR, pp 9376–9385
- Xie GS, Liu L, Jin X, Zhu F, Zhang Z, Yao Y, Qin J, Shao L (2020) Region graph embedding network for zero-shot learning. In: ECCV
- Xu W, Xian Y, Wang J, Schiele B, Akata Z (2020) Attribute prototype network for zero-shot learning. In: NeurIPS
- Xu W, Xian Y, Wang J, Schiele B, Akata Z (2022) Attribute prototype network for any-shot learning. International Journal of Computer Vision 130:1735 – 1753
- Yang X, Zhang H, Qi G, Cai J (2021) Causal attention for vision-language tasks. In: CVPR, pp 9842–9852
- Yu H, Lee B (2019) Zero-shot learning via simultaneous generating and learning. In: NeurIPS
- Yu Y, Ji Z, Han J, Zhang Z (2020) Episode-based prototype generating network for zero-shot learning. In: CVPR, pp 14032–14041
- Yue Z, Zhang H, Sun Q, Hua X (2020) Interventional few-shot learning. In: NeurIPS

- Yue Z, Wang T, Zhang H, Sun Q, Hua X (2021) Counterfactual zero-shot and open-set visual recognition. In: CVPR
- Zhai Y, Ye Q, Lu S, Jia M, Ji R, Tian Y (2020) Multiple expert brainstorming for domain adaptive person re-identification. In: ECCV
- Zhang Y, Xiang T, Hospedales TM, Lu H (2018) Deep mutual learning. In: CVPR, pp 4320–4328
- Zhang Y, Gong M, Liu T, Niu G, Tian X, Han B, Scholkopf B, Zhang K (2021) Causaladv: Adversarial robustness through the lens of causality. In: ICLR
- Zhou K, Yang J, Loy CC, Liu Z (2022) Learning to prompt for vision-language models. *International Journal of Computer Vision* 130:2337 – 2348
- Zhu Y, Xie J, Tang Z, Peng X, Elgammal A (2019) Semantic-guided multi-attention localization for zero-shot learning. In: NeurIPS